X-652-73-269
PREPRINT

MICROWAVE MAPS OF THE POLAR ICE OF THE EARTH

P. GLOERSEN
T. T. WILHEIT
T. C. CHANG
W. NORDBERG
W. J. CAMPBELL

AUGUST 1973

GODDARD SPACE FLIGHT CENTER
GREENBELT, MARYLAND

X-652-73-269
Preprint

MICROWAVE MAPS OF THE POLAR ICE OF THE EARTH

P. Gloersen, T. T. Wilheit, T. C. Chang, and W. Nordberg
Goddard Space Flight Center
Greenbelt, Maryland

and

W. J. Campbell
Ice Dynamics Project, U.S.G.S.

August 1973

GODDARD SPACE FLIGHT CENTER
Greenbelt, Maryland

MICROWAVE MAPS OF THE POLAR ICE OF THE EARTH

P. Gloersen, T. T. Wilheit, T. C. Chang, and W. Nordberg

Goddard Space Flight Center

Greenbelt, Maryland

and

W. J. Campbell

Ice Dynamics Project, U.S.G.S.

ABSTRACT

Synoptic views of the entire polar regions of Earth have been obtained free of the usual persistent cloud cover using a scanning microwave radiometer operating at a wavelength of 1.55 cm on board the Nimbus-5 satellite. Three different views at each pole are presented utilizing data obtained at approximately one-month intervals during the winter of 1972-1973. The major discoveries resulting from an analysis of these data are as follows: 1) Large discrepancies exist between the climatic norm ice cover depicted in various atlases and the actual extent of the canopies. 2) The distribution of multiyear ice in the north polar region is markedly different from that predicted by existing ice dynamics models. 3) Irregularities in the edge of the Antarctic sea ice pack occur that have neither been observed previously nor anticipated. 4) The brightness temperatures of the Greenland and Antarctica glaciers show interesting contours probably related to the ice and snow morphologic structure.

CONTENTS

BACKGROUND

The Electronically-Scanned Microwave Radiometer (ESMR) used for obtaining the measurements to be described here has been discussed in detail elsewhere (Wilheit, 1972). It consists of a Dicke-type radiometer (Dicke, 1946) with a temperature sensitivity of 2 K fed by a phased-array antenna which step-scans across the subsatellite track in 78 beam positions by means of ferrite phase shifters contained in the antenna elements. The total swath covered is ±50° from nadir. The radiometric data are telemetered orbit-by-orbit, along with internal calibration data, and are computer-processed into the format presented in this paper. Approximately one day's worth of data are accumulated for one polar projection; redundant data in a given map cell, resulting from orbit swath overlap, are averaged for that time period. Brightness temperatures, which are directly proportional to the received radiometric power since the Rayleigh-Jeans approximation applies, are assigned various colors so as to produce a false-color image. The resolution cell size in the processed image is 32 Km.

The brightness temperatures observed with the ESMR in general depend on the physical temperature and emissivity of the surface and the opacity and temperature profile of the intervening atmosphere. However, the atmospheric contributions in the polar regions are generally negligible due to the low humidity and near absence of liquid water droplets in these regions (Wilheit et al., 1972). The cloud cover generally consists of low-altitude stratus clouds, whose liquid

water content is too small to affect the microwave emission. The ice crystals contained in cirrus clouds are quite transparent to the 1.55 cm radiation.

The surface emissivity accounts for the largest signal contrast observed in the polar regions; however, variations in the physical temperature of the surface are observed also. At 1.55 cm, the emissivity of sea water is about 0.4, for first-year sea ice it is about 0.95, and for multiyear ice it is about 0.8 (Wilheit et al., 1972, Gloersen et al., 1973). Thus, in the presence of first-year ice only, the fraction of F of unresolved open water in a given resolution cell may be determined from the following expression:

$$F = (T_B - 0.95\,T_S)/(T_W - 0.95\,T_S)$$

where T_B is the brightness temperature observed at 1.55 cm, T_S is the thermodynamic temperature of the ice surface, and T_W is the brightness temperature of smooth open water. T_S may be assumed to be the seasonal average ±10 K and T_W is 131 ±5 K (Wilheit et al., 1972). If T_B is measured to within 2 K, the uncertainties in T_S and T_W lead to an accuracy of the determination of the fractional open water, F, to within 6 percentage points.

It has been suggested that the assumed emissivity for first-year ice (0.95) may not be correct for temperatures within 10 K of the melting point of the first-year sea ice (Edgerton et al., 1971). However, radiometric data obtained from aircraft flights over Arctic sea ice in the summer (Wilheit et al., 1972) are consistent with an emissivity of 0.95 for first-year ice, based on encounters with surface temperatures within 2 K of the melting point as determined with an onboard infrared radiometer.

ICE PACK BOUNDARY MEASUREMENTS

A comparison between the predicted and actual boundaries of the polar ice packs for three different time periods is given in Plates 1-6 and opposing Figures 1-6. The predictions were based (Daniel, 1957 and 1958) on available ship and aircraft reports; for Antarctica, the information is substantially the same in several atlases, published both in the Soviet Union and in the U.S.A. In comparing our actual measurements of the ice boundaries with the predictions, it is of course recognized that there are trends in the state of the ice cover that cannot be covered in the atlases and that the predictions are based upon long past seasons. The purpose of the comparison is to illustrate that large differences exist between the actual ice edge and the climatic norm.

In the Arctic, probably the most striking observation is that during the 1972-3 season much more ice cover was observed in the East Greenland Sea than is estimated in the atlas. Off northern Greenland, the ice extends more than 4° longitude further eastward than expected for two of the three time periods illustrated. On the other hand, the seas north of Svalbard and southeast of Greenland are shown as ice-covered in the atlases but are actually open, as shown in the microwave images. Finally, freezing of the waters in the Northern Baffin Bay, the White Sea, the Chukchi Sea, Bering Strait, and the Bering Sea occurred later during the 1972-3 winter than is predicted by the atlases.

The differences noted in the Antarctic between climatic data and the 1972-3 observations are even more striking, particularly in the Ross and Weddell Seas

where the observed ice cover is consistently less solid than shown in the atlas. For instance, according to the atlas the Ross Sea is never completely open to the South Pacific. Observations on both January 11 and 30 (Plates 5 and 6) show that the ice cover is less than 15% at the Ross Sea-Pacific boundary. In mid-December, there is considerable open water off the Ross Ice shelf, when the atlas would lead one to expect a 50-80% cover at that time. Such disparity between the synoptic observation via Nimbus-5 and the statistical prediction of the atlases aptly illustrates the need to observe sea ice distribution over large space scales at small time scales in order to develop and test dynamic rather than statistical models for more accurate forecasting. It is interesting also that the minimum ice cover that is climatically expected for the shore along Coats Land is greater than 50%, whereas it was observed to be less than 15% on January 30, 1973. Perhaps the most obvious difference between the observed and predicted ice boundaries of the Antarctic is that the observations, especially for mid-December, show large irregular perturbations around the ice edge whereas the seasonal averages in the atlases show smooth edges. These irregularities are new knowledge, unforeseen by statistics or intuition. So far, all of these observations are, of course, just for one particular season of one year. If Nimbus-5 and the ESMR meet or exceed their design lifetimes, we will be in a position to map these changes for a complete year and perhaps much more accurate statistics can be derived from similar observations in future years.

There are also indicated uncertainties in the shoreline of Antarctica (Daniels, 1957). An overlay of the atlas data on the ESMR image indicates discrepancies of several resolution elements at various places along the coastline. A judicious combination of ESMR maps and surface information may facilitate improvement of the accuracy of the coastline determination.

ICE PACK DENSITY AND ICE DYNAMICS OBSERVATIONS

In Antarctica, there are two features of particular interest. First, the long finger of ice, less than 50% cover, that stretches out from the Palmer Peninsula and almost closes off the Weddell Sea on December 16, 1973 drifted about 8° due north by January 11, and was out of the field of view by January 30. The second interesting feature is the nature of the opening of the Ross Sea and the shoreline along Marie Byrd Land and the Ellsworth Highland. A distinct impression of a tearing away of the ice pack from the continent is given as the amount of open water progressively increases along the shoreline in the series of three scenes (Plates 4-5). In the case of the Ross Sea ice pack, the displacement of the jigsaw puzzle-like edge of the pack from the shoreline is suggestive of a shearing induced by a prevailing local wind. Although surface wind observations on the Ross Ice Shelf are not available for this period, sufficient studies have been made (Rubin, 1959) to reveal a close correlation between the katabatic winds draining seaward off the shelf and the observed winds at McMurdo Station. These katabatic winds can be strong, with average wind velocities of about 25 knots for periods as long as several days to a week. During December 1972 and January 1973, the surface isobaric charts and wind records indicate that several

periods of intense katabatic activity occurred on the Ross Ice Shelf. It appears that the katabatic winds strip the ice away from the shelf edge and transport it northward. The ambient surface wind flow on the Ross Sea during December 1972 was from the east. Thus, the ice distribution in the Ross Sea shown in Plate 4 results apparently from a combination of the southerly katabatic winds flowing off the Shelf and the ambient eastward winds acting on the ice north of the Shelf.

The U.S. Navy Atlas (Daniel, 1957) shows such a prevailing wind for November, but data were not available for December or January. The prevailing wind for February is shown as reversed, consistent with the apparent tearing away of the remaining pack ice from the shoreline of Marie Byrd Land.

The Arctic ice canopy, especially in the shear zones, is subject to large variations in the density in the pack. This will probably become more evident later when more than three synoptic views become available, but even in the views shown here (Plates 1-3) there is evidence of the pack in the East Laptev Sea becoming less dense as winter progresses, and as the ice in the Beaufort Sea becomes more consolidated. Changes in the consolidation of the pack ice in the Bering Sea are easily discerned in these three views, also, but since the ambient temperature is steadily decreasing, the observation may be related simply to the in situ freezing of the ice pack. The gradual decrease in the consolidation of the pack with distance off the eastern shore of Greenland is readily seen; the ice is 100% consolidated along the shoreline (yellows and greens in

Plates 1-3), has some patches of less than 20% open (light blue) throughout, is largely 20% open for most of the area (blue), has some fringed areas of about 35% open near the edge (dark blue), and at the very edge has some areas of 50% open water (darker grey). The accuracy of the determinations directly from these false-color images is approximately ±6% points based on the assumption that the bulk of the ice is first-year. Multiyear ice in this area injected by the Trans-Polar Drift Stream could affect these estimates, but the amount of multiyear ice so injected is unknown and assumed to be small. A large number of changes in this distribution are evident in the series of three plates.

DISTRIBUTION OF MULTIYEAR ICE IN THE ARCTIC

The similarity of the average brightness temperature for multiyear ice and first-year ice with 20% open water on Plates 1-3 makes it difficult to determine the extent of multiyear ice coverage on a prima facie basis. Ultimately, when a full year's data become available, this task will become easier, since the ice that persists through a summer is by definition multiyear ice, and initial boundaries can be established which can be traced forwards or backwards into time. For the time being, we must be content to speculate on the basis of some very limited aircraft (Gloersen et al., 1973, Campbell et al., 1973) and surface data (Hibler et al., 1973) accumulated over the Beaufort Sea and some qualitative knowledge of the ice dynamics in the Beaufort Sea. Perhaps the most surprising result is the finger of multiyear ice that apparently extends south to about 72°N in the Eastern Beaufort Sea. Such a southward extension of the multiyear ice

was not expected on the basis of most current ice dynamics models (Rothrock, 1973). Support for these observations has been obtained recently also from ERTS-1 imagery (Campbell et al., 1973).

CONTINENTAL ICE

Brightness temperatures measured over Greenland and Antarctica are lower than over any surface on Earth except for open water. They range from 130 to 160°K over the interior of Antarctica and from 155 to 200°K over Greenland.

In Antarctica, the brightness temperature patterns are related strongly, although not entirely, to the horizontal distribution of physical temperatures in the upper layer of the continental ice sheet, as determined from climatic records. This is not the case for Greenland, however, where the lowest brightness temperatures (155°K) are measured over the northern and southwestern portions. In those regions, the elevation of the ice sheet is lower (and the surface temperature is therefore probably higher) than the center of the ice plateau where about 40°K higher brightness temperatures are observed.

The emissivities inferred from these measurements over Greenland and Antarctica and from climatic records of upper layer temperatures range from 0.65 to 0.75, except for some Antarctic glaciers, especially the Lambert Glacier, and the Amery, Ross, and Filchner Ice Shelves which have an emissivity of about 0.8. Generally higher emissivities, namely 0.75, 0.85, and 0.95 obtained over the South Cascade Glacier in the North Cascade Mountains, Washington (Schmugge et al., 1974), over multiyear sea ice (Wilheit et al., 1973,

Gloersen et al., 1973), and over first-year sea ice (ibid.), respectively. These latter emissivities were derived from airborne radiometer measurements at 1.55 cm and 11 micrometers during the winters of 1971/72 and 1970/71. We believe that these differing emissivities must be attributed to varying crystaline forms, amounts of entrapped air, depth and frequency of fissures, and, at least in the case of sea ice, amounts of entrapped brine in the freeboard layer.

A preliminary analysis of the Antarctic and Greenland ice sheet emissivities derived from the ESMR measurements shows that they are practically constant for the period from December 1972 to July 1973. We conclude, therefore, that this invariance of emissivities with seasons is a further indication that they are correlated primarily with structural rather than with temperature variations in the ice.

CONCLUSIONS

We have shown here some of the early results from the data acquired by the ESMR on board the Nimbus-5 satellite. It is clear that imaging thermally emitted microwaves with satellites is a powerful tool for studying sea ice coverage, type, and distribution in the polar areas of Earth. The independence of this technique from cloud cover in the polar regions will permit a detailed study of the sea ice characteristics as a function of time. The ESMR images are already being used operationally as an aid to navigation in polar waters (Ellinghausen, 1973). More analysis will be done when a larger data base has been acquired. Work in progress includes a more precise determination of the actual extent of

the multiyear ice pack in the Arctic, observations of the ice pack motion on a longer time scale using smaller time intervals, a study of the open water distribution as a function of time, and finally a test of the consequences of utilizing the open water distribution information in a global weather model study. It is hoped that the early results presented here will inspire others to conceive still other applications of these data.

REFERENCES

Campbell, W. J., P. Gloersen, W. Nordberg, and T. T. Wilheit, Dynamics and morphology of Beaufort Sea ice determined from satellites, aircraft, and drifting stations, Paper No. A.5.6, Proc. of the Symp. on Approaches to Earth Sciences through the Use of Space Technology, COSPAR WG6 (1973).

Daniel, H. C., Oceanographic atlas of the polar seas, U.S. Navy Hydrographic Office Publication No. 705; Part I Antarctic (1957), Part II Arctic (1958).

Dicke, R. H., The measurement of thermal radiation at microwave frequencies, Rev. Sci. Inst. 17, 280 (1946).

Edgerton, A. T., A. Stogryn, D. P. Williams, and G. Poe, A study of the microwave emission characteristics of sea ice, Summary Report 1741R-2, NOAA/NESS Contract No. 1-35139 (1971).

Ellinghausen, W. A., Priv. comm. (1973) (U.S. Navy Fleet Facility Service.)

Gloersen, P., W. Nordberg, T. J. Schmugge, T. T. Wilheit, and W. J. Campbell, Microwave signatures of first-year and multiyear sea ice, J. Geoph. Res. 78, 3564 (1973).

Hibler, W., W. Weeks, S. Ackley, A. Kovacs, and W. Campbell, Mesoscale strain measurements on the Beaufort Sea pack ice, J. Glaciol., in press, 1973.

Rothrock, D., The steady drift of an incompressible ice cover in the Arctic Ocean, Proc. of Climate of the Arctic, 24th Alaska Science Conference (1973) In Press.

Rubin, M. J., Advection across the Antarctic boundary, Proceedings of the Antarctic Meteorology Symposium held in Melbourne (1959).

Schmugge, T., T. T. Wilheit, P. Gloersen, M. F. Meier, D. Frank, and I. Dirnhirm, Microwave signatures of snow and fresh water ice, Paper No. 5.12, Proc. of the Interdisciplinary Symp. on Adv. Concepts and Techniques in the Study of Snow and Ice Resources, Asilomar (To be published in 1974).

Wilheit, T. T., The electronically scanning microwave radiometer (ESMR), pp. 59-104, The Nimbus 5 User's Guide, U.S. Government Printing Office 1972-735-963/259 (1972).

Wilheit, T. T., W. Nordberg, J. Blinn, W. Campbell, and A. Edgerton, Aircraft measurements of microwave emission from Arctic sea ice, Remote Sensing of Environment 2, 129 (1973).

Plate 1. False-color polar projection map of 1.55-cm microwave radiometer data obtained on December 16, 1972 from the Nimbus-5 satellite in the vicinity of the North Pole. Greenland appears in the lower center of the image.

Figure 1. Comparison of part of the data in Plate 1 (ESMR) with predictions based on data from the same month in the USN Polar Atlas (Daniel). The indicated edge of the ice pack was used in both cases.

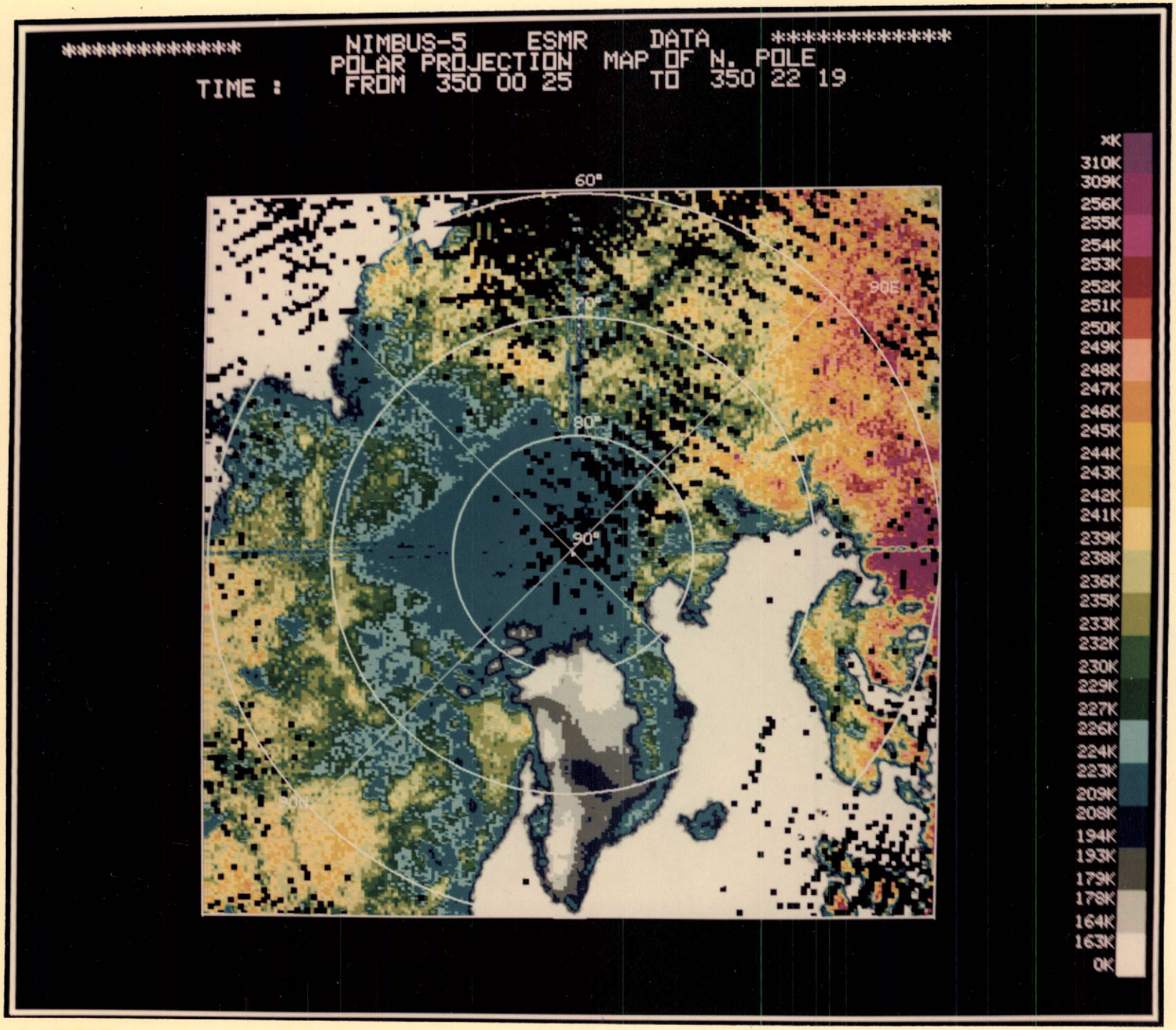
NIMBUS-5 ESMR DATA
POLAR PROJECTION MAP OF N. POLE
TIME : FROM 350 00 25 TO 350 22 19
60°
70°
80°
90°
90E
90N
xK
310K
309K
256K
255K
254K
253K
252K
251K
250K
249K
248K
247K
246K
245K
244K
243K
242K
241K
239K
238K
236K
235K
233K
232K
230K
229K
227K
226K
224K
223K
209K
208K
194K
193K
179K
178K
164K
163K
0K

SEA-ICE BOUNDARIES
DECEMBER

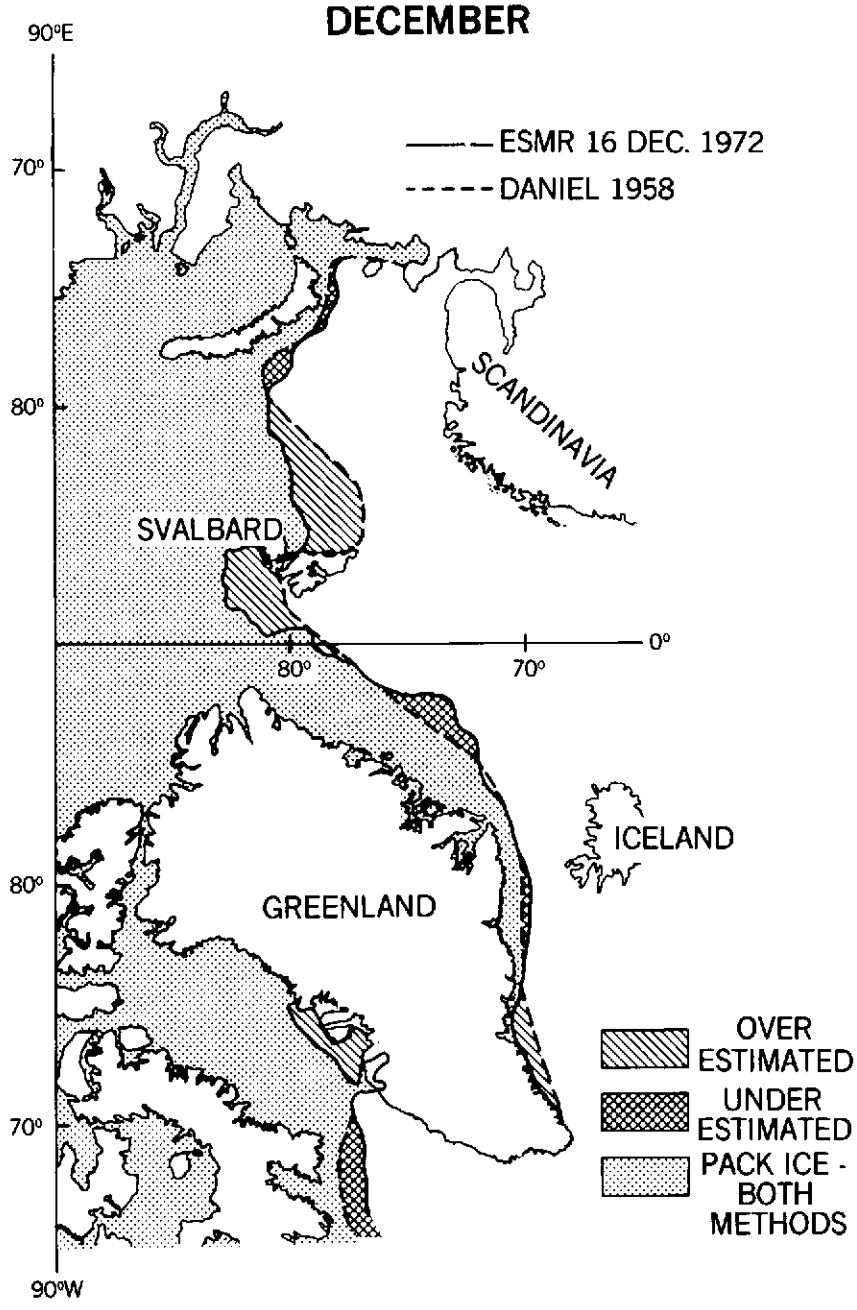

Page intentionally left blank

Plate 2. False-color polar projection map of 1.55-cm microwave radiometer data obtained on January 11, 1973 from the Nimbus-5 satellite in the vicinity of the North Pole. Greenland appears in the lower center of the image.

Figure 2. Comparison of part of the data in Plate 2 (ESMR) with predictions based on data from the same month in the USN Polar Atlas (Daniel). The indicated edge of the ice pack was used in both cases.

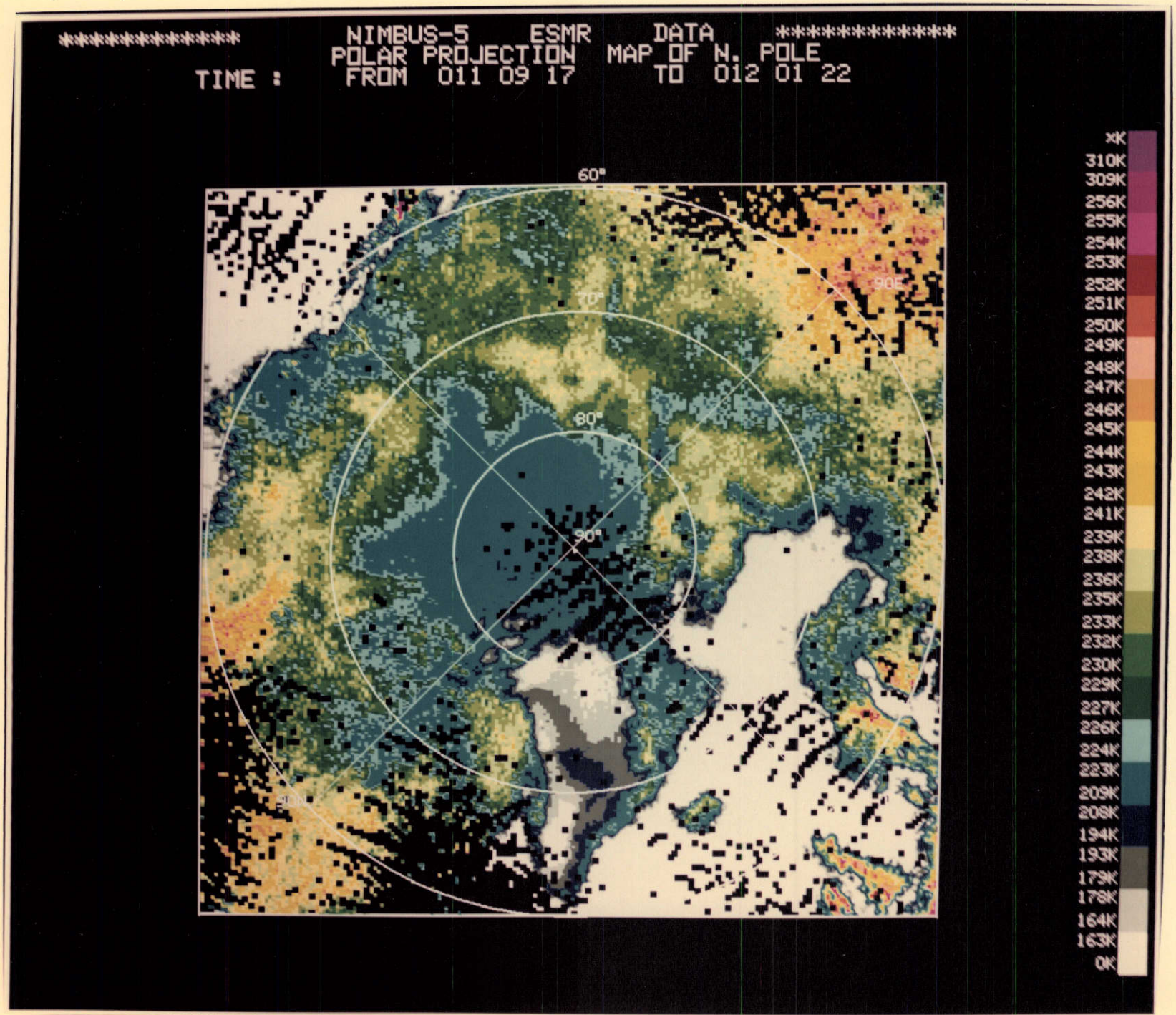
NIMBUS-5 ESMR DATA
POLAR PROJECTION MAP OF N. POLE
TIME : FROM 011 09 17 TO 012 01 22
60°
70°
80°
90°
90°
90°
xK
310K
309K
256K
255K
254K
253K
252K
251K
250K
249K
248K
247K
246K
245K
244K
243K
242K
241K
239K
238K
236K
235K
233K
232K
230K
229K
227K
226K
224K
223K
209K
208K
194K
193K
179K
178K
164K
163K
0K

SEA-ICE BOUNDARIES

JANUARY

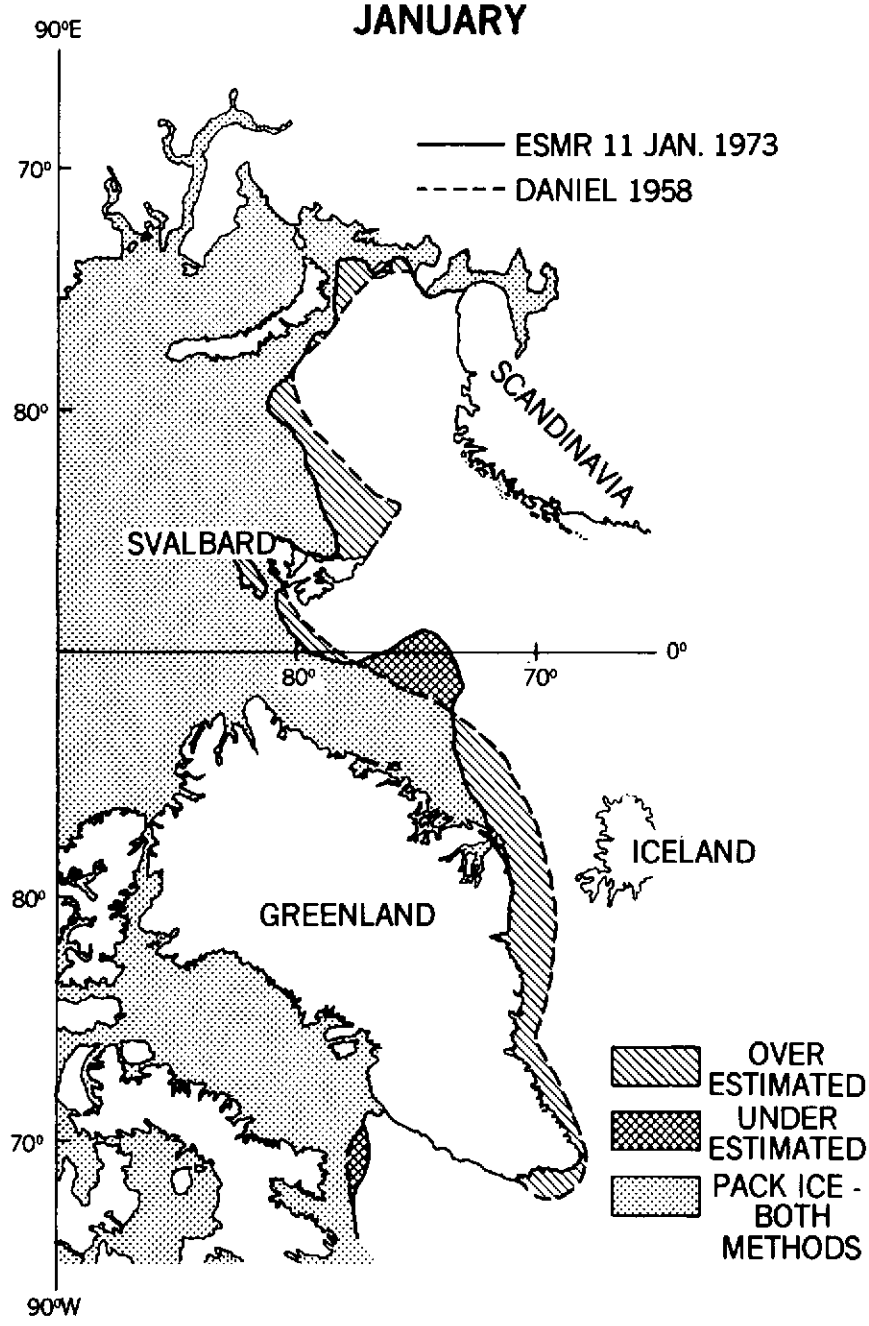

Page intentionally left blank

Plate 3. False-color polar projection map of 1.55-cm microwave radiometer data obtained on February 10, 1973 from the Nimbus-5 satellite in the vicinity of the North Pole. Greenland appears in the lower center of the image.

Figure 3. Comparison of part of the data in Plate 3 (ESMR) with predictions based on data from the same month in the USN Polar Atlas (Daniel). The indicated edge of the ice pack was used in both cases.

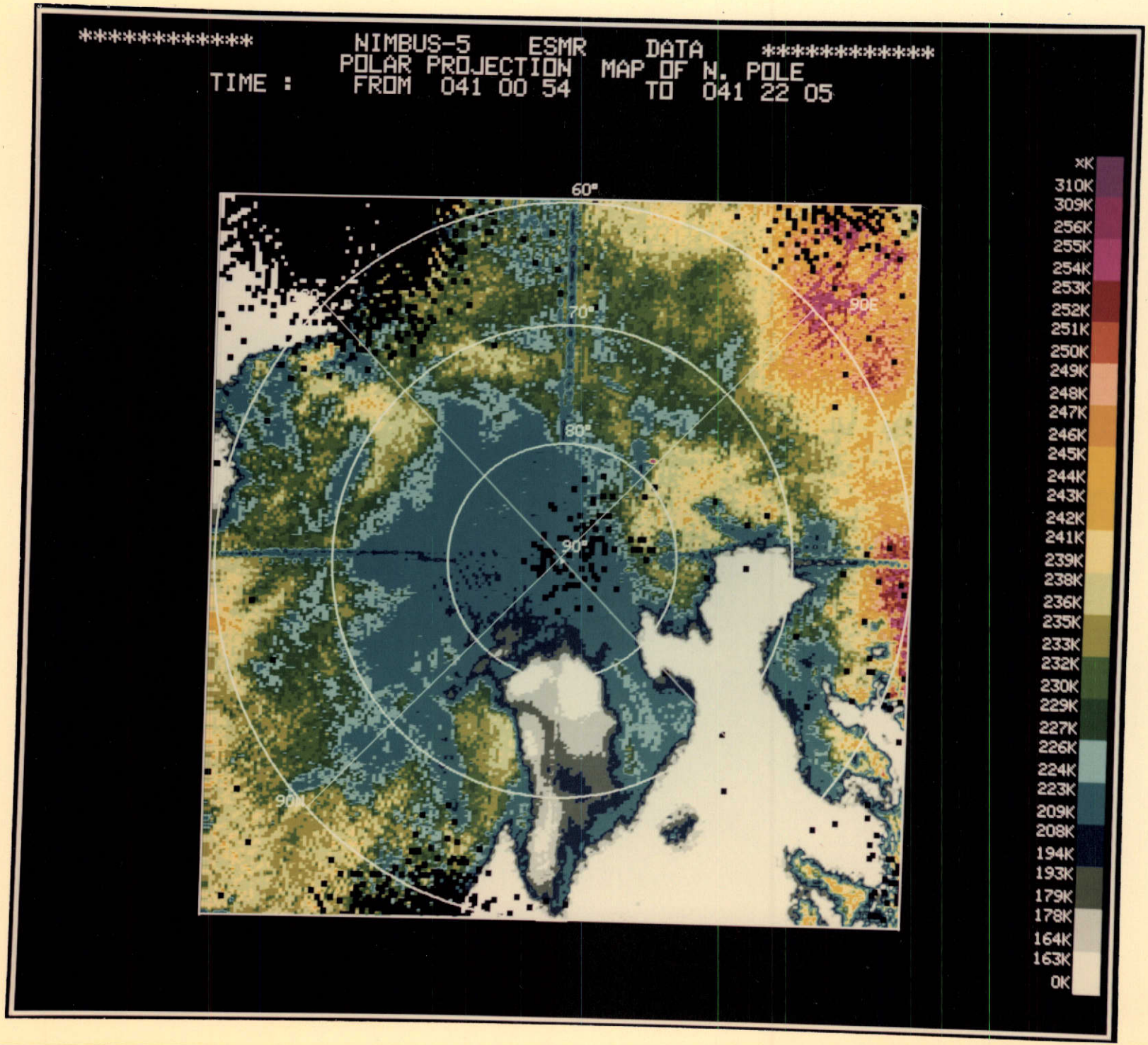
********** NIMBUS-5 ESMR DATA **********
POLAR PROJECTION MAP OF N. POLE
TIME : FROM 041 00 54 TO 041 22 05
60°
70°
80°
90°
90E
90W
xK
310K
309K
256K
255K
254K
253K
252K
251K
250K
249K
248K
247K
246K
245K
244K
243K
242K
241K
239K
238K
236K
235K
233K
232K
230K
229K
227K
226K
224K
223K
209K
208K
194K
193K
179K
178K
164K
163K
0K

SEA-ICE BOUNDARIES
FEBRUARY

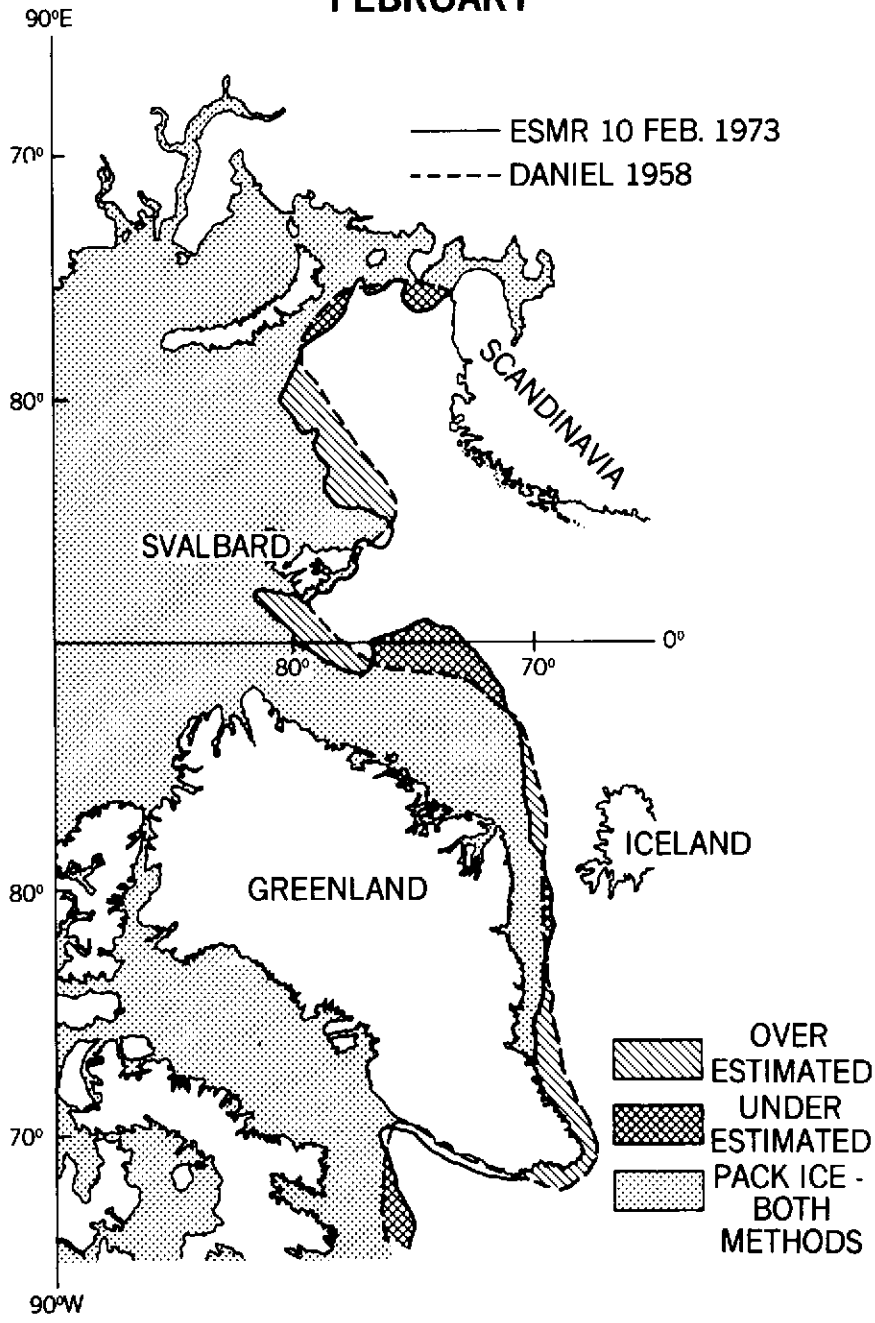

Page intentionally left blank

Plate 4. False-color polar projection map of 1.55-cm microwave radiometer data obtained on December 16, 1972 from the Nimbus-5 satellite in the vicinity of the South Pole. The white area enclosed in the upper right corner of Antarctica is open water in the Ross Sea between the Ross Ice Shelf and the sea ice pack.

Figure 4. Comparison of part of the data in Plate 4 (ESMR) with predictions based on data from the same month in the USN Polar Atlas (Daniel). The indicated edge of the ice pack was used in both cases.

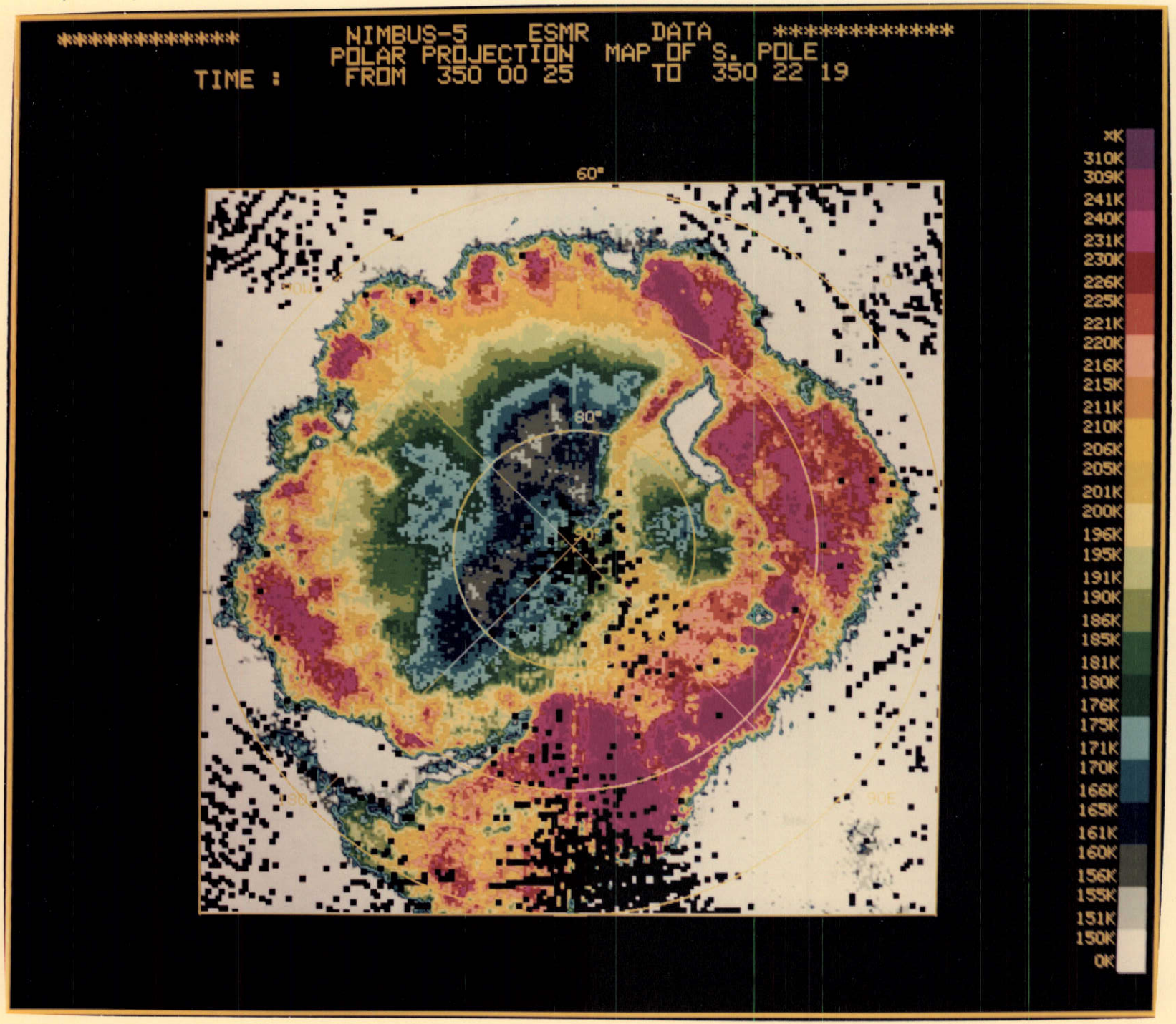
NIMBUS-5 ESMR DATA
POLAR PROJECTION MAP OF S. POLE
TIME : FROM 350 00 25 TO 350 22 19
60°
80°
90°
xK
310K
309K
241K
240K
231K
230K
226K
225K
221K
220K
216K
215K
211K
210K
206K
205K
201K
200K
196K
195K
191K
190K
186K
185K
181K
180K
176K
175K
171K
170K
166K
165K
161K
160K
156K
155K
151K
150K
0K

SEA-ICE BOUNDARIES
DECEMBER

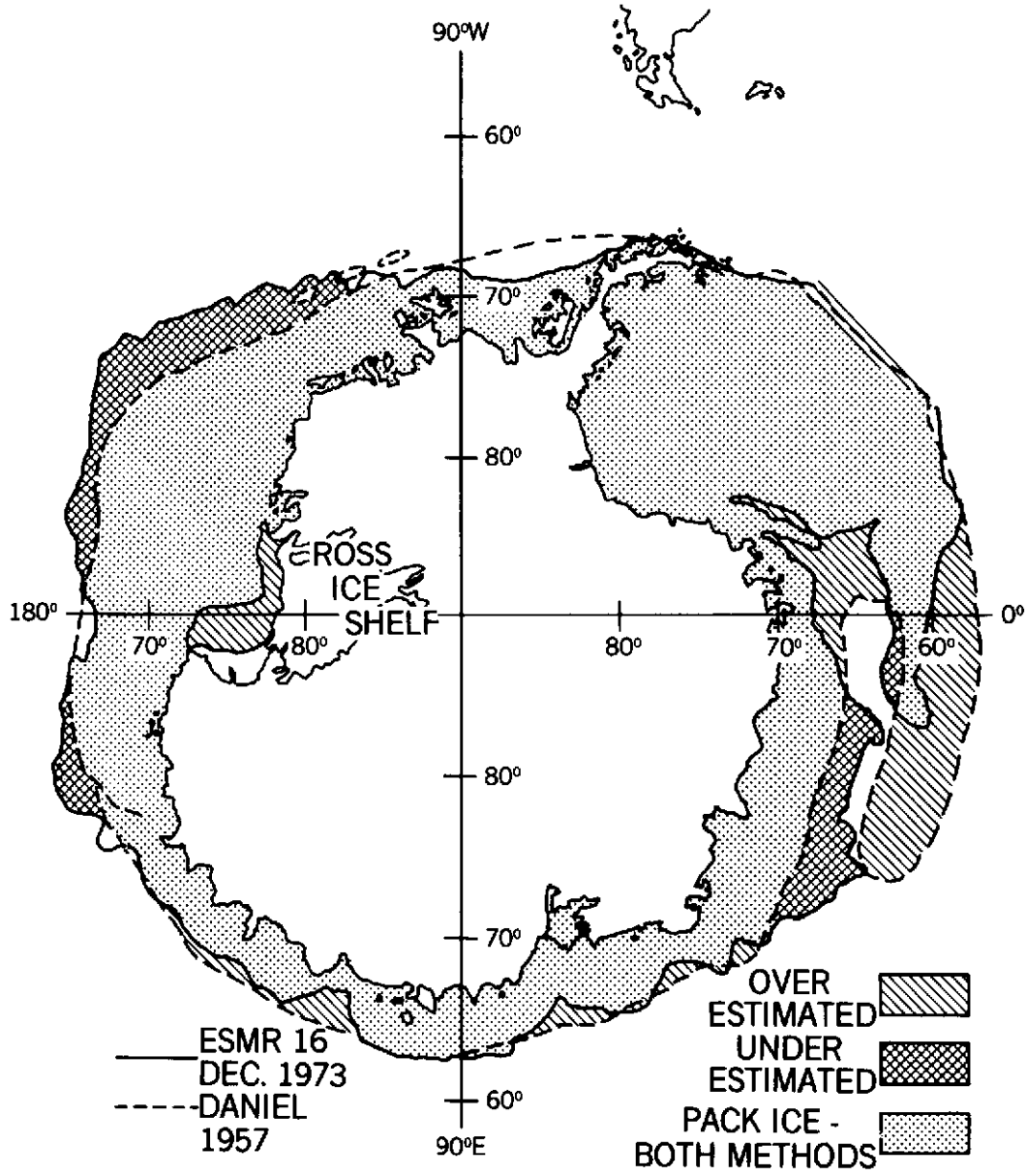

Page intentionally left blank

Plate 5. False-color polar projection map of 1.55-cm microwave radiometer data obtained on January 11, 1973 from the Nimbus-5 satellite in the vicinity of the South Pole. The white area enclosed in the upper right corner of Antarctica is open water in the Ross Sea between the Ross Ice Shelf and the sea ice pack.

Figure 5. Comparison of part of the data in Plate 5 (ESMR) with predictions based on data from the same month in the USN Polar Atlas (Daniel). The indicated edge of the ice pack was used in both cases.

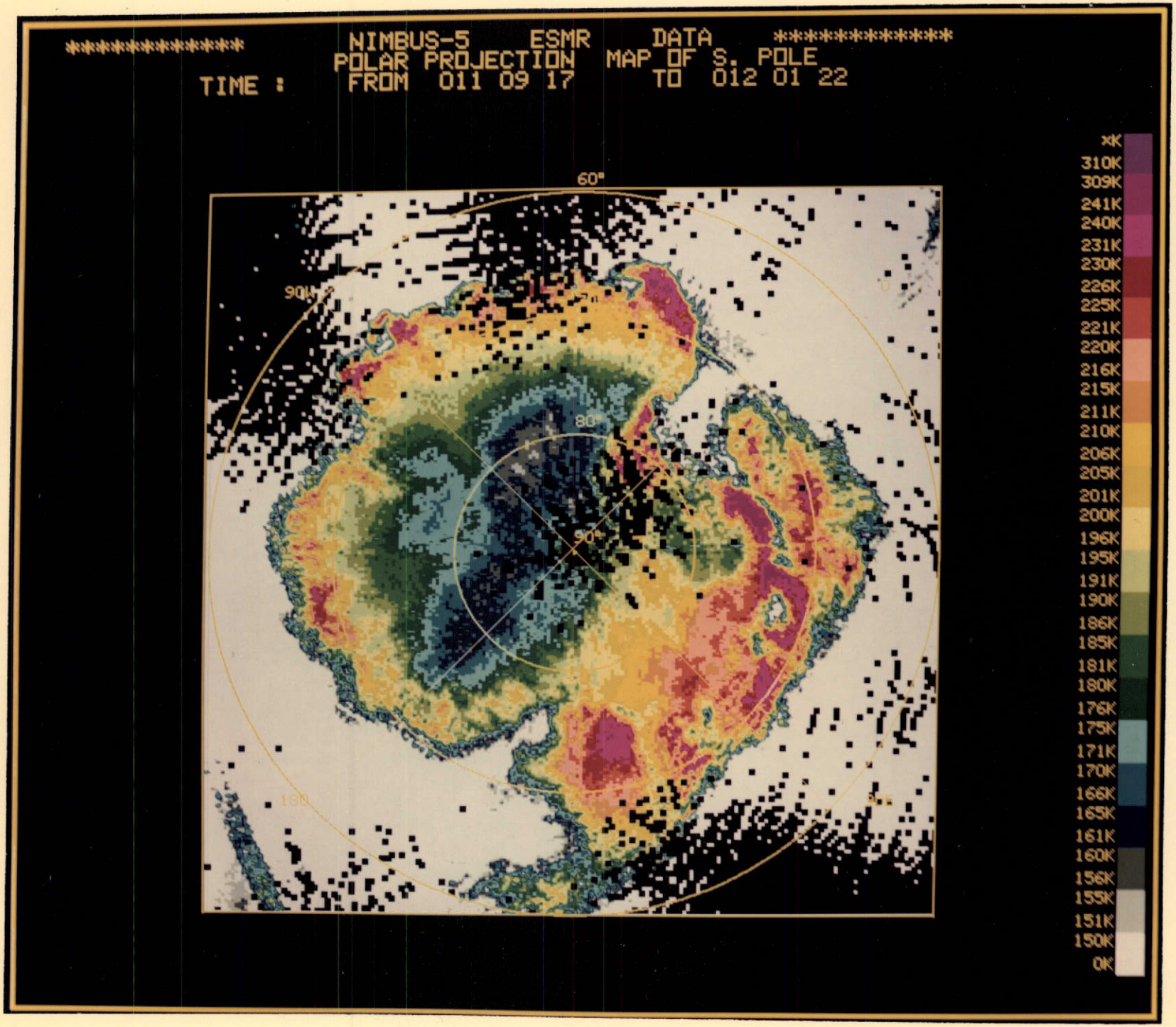
NIMBUS-5 ESMR DATA
POLAR PROJECTION MAP OF S. POLE
TIME : FROM 011 09 17 TO 012 01 22
60°
90W
80°
90°
180
0
90E
xK
310K
309K
241K
240K
231K
230K
226K
225K
221K
220K
216K
215K
211K
210K
206K
205K
201K
200K
196K
195K
191K
190K
186K
185K
181K
180K
176K
175K
171K
170K
166K
165K
161K
160K
156K
155K
151K
150K
0K

SEA-ICE BOUNDARIES

JANUARY

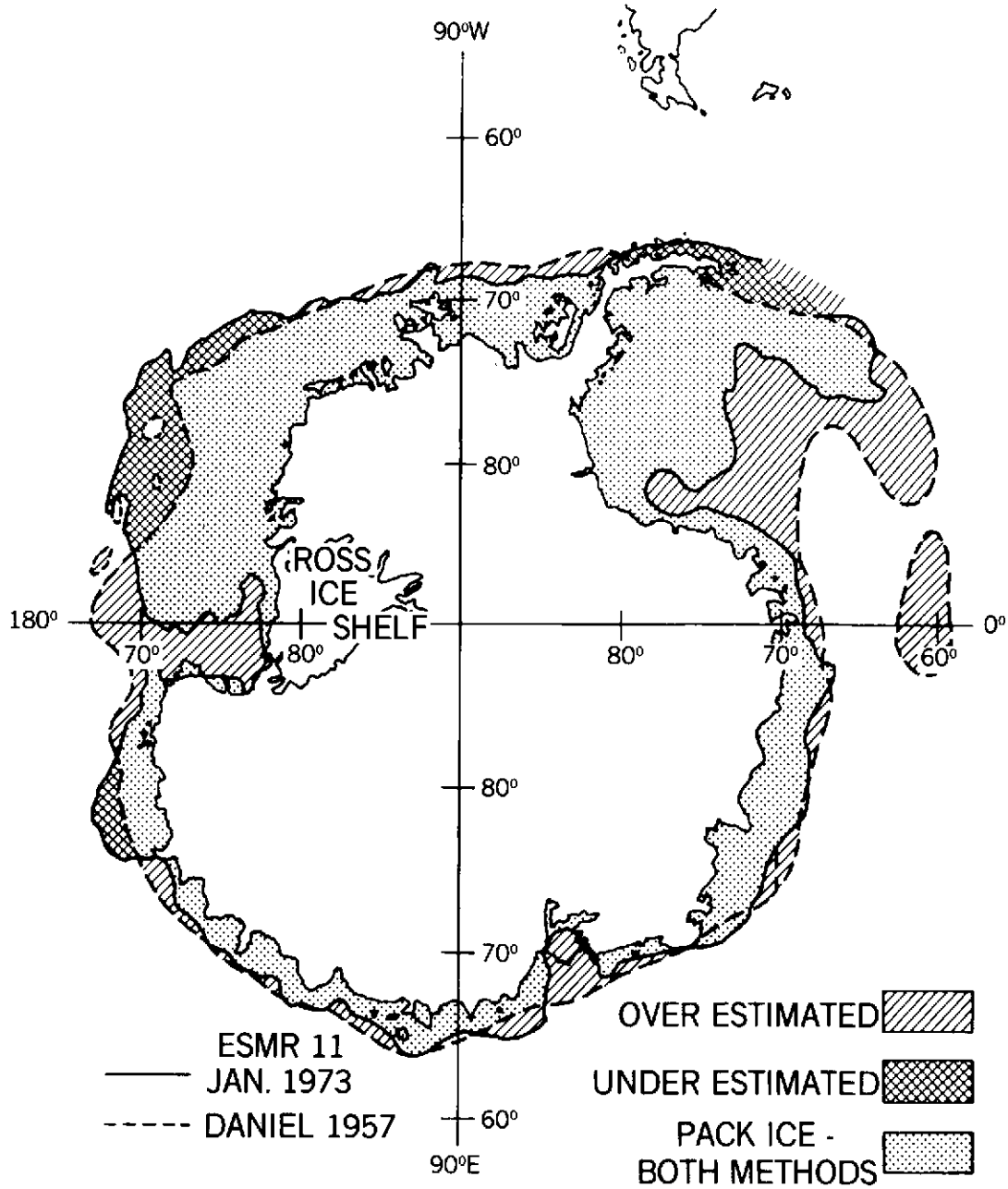

Page intentionally left blank

Plate 6. False-color polar projection map of 1.55-cm microwave radiometer data obtained on January 30, 1973 from the Nimbus-5 satellite in the vicinity of the South Pole. The white area enclosed in the upper right corner of Antarctica is open water in the Ross Sea between the Ross Ice Shelf and the sea ice pack.

Figure 6. Comparison of part of the data in Plate 6 (ESMR) with predictions based on data from February in the USN Polar Atlas (Daniel). The indicated edge of the ice pack was used in both cases.

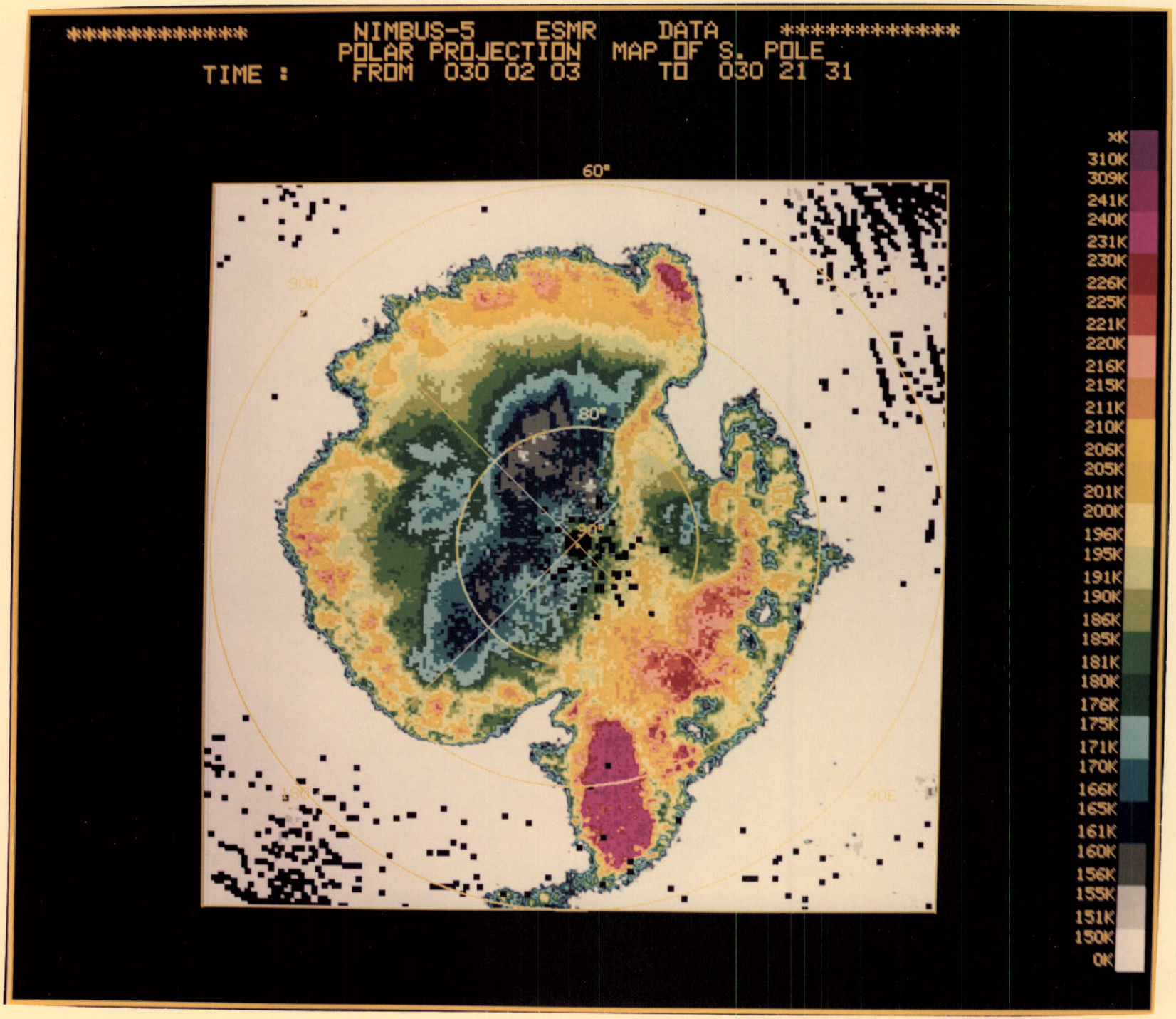
NIMBUS-5 ESMR DATA
POLAR PROJECTION MAP OF S. POLE
TIME : FROM 030 02 03 TO 030 21 31
60°
80°
90°
90W
90E
xK
310K
309K
241K
240K
231K
230K
226K
225K
221K
220K
216K
215K
211K
210K
206K
205K
201K
200K
196K
195K
191K
190K
186K
185K
181K
180K
176K
175K
171K
170K
166K
165K
161K
160K
156K
155K
151K
150K
0K

SEA-ICE BOUNDARIES
FEBRUARY

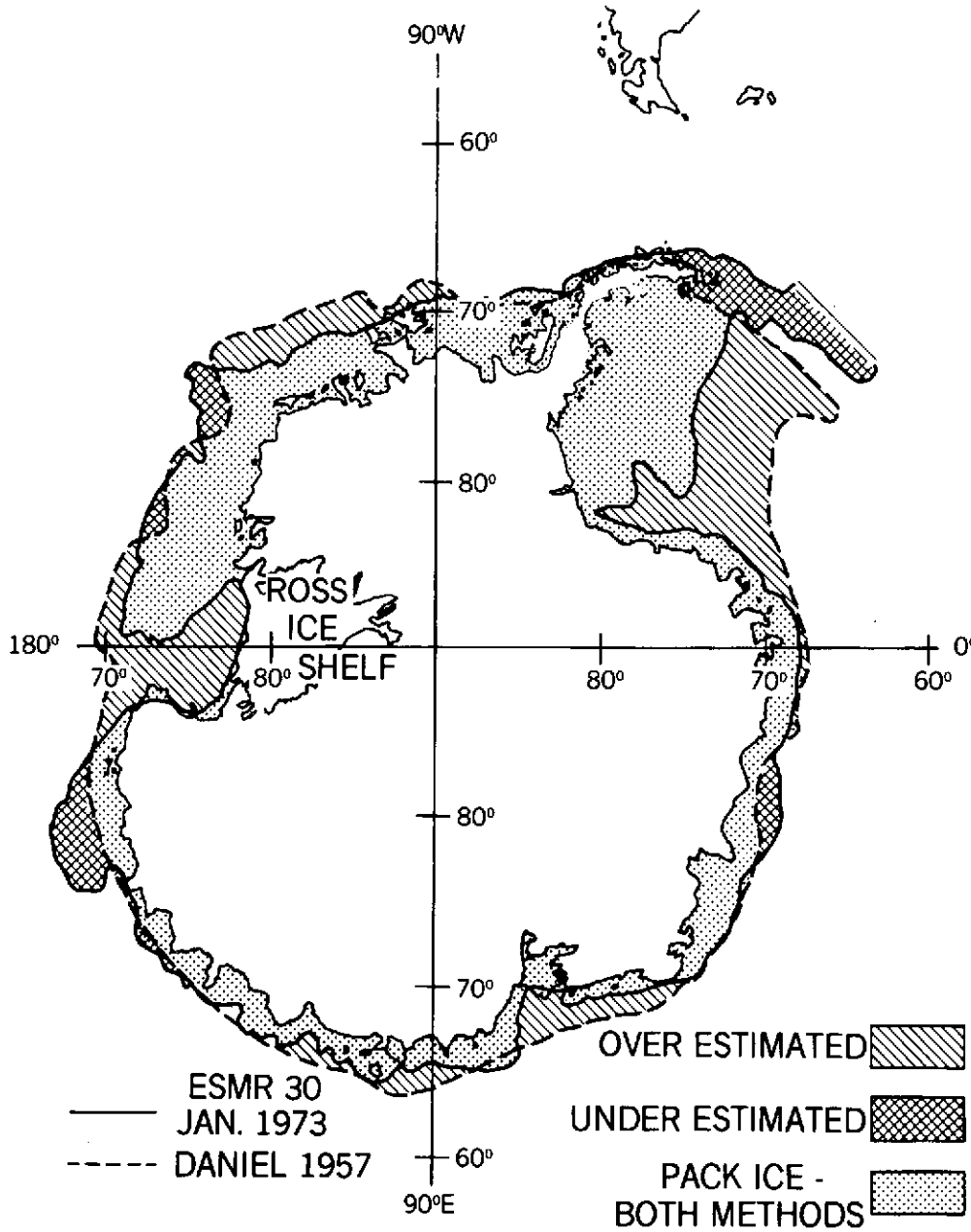

Page intentionally left blank

Plate 7. Seasonal variations of the brightness temperatures over the continental ice sheets in Greenland and Antarctica.

GREENLAND

(G)

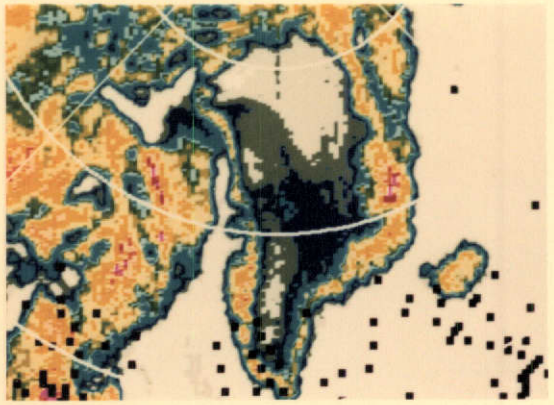

21 JUNE 1973

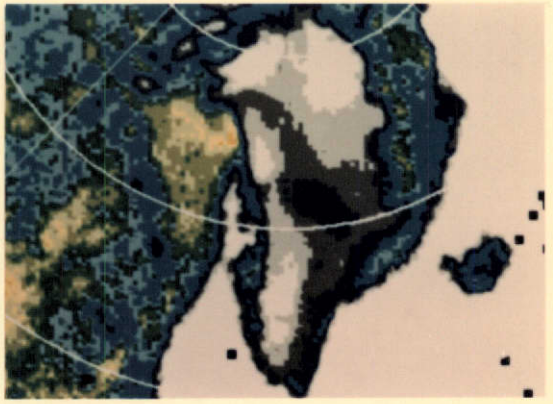

15 DEC. 1972

ANTARCTICA

(A)

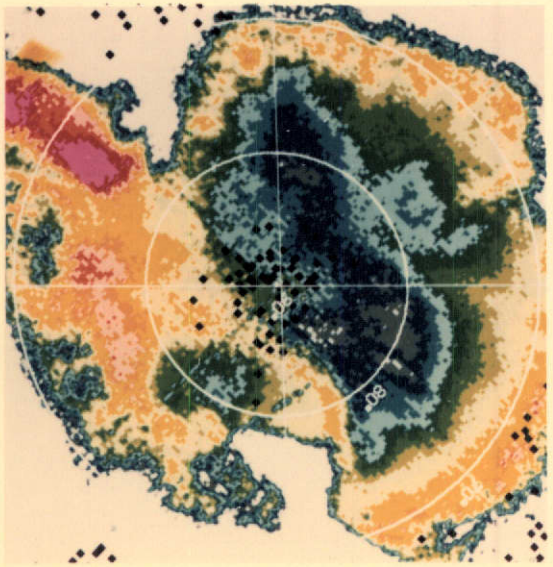

10 FEB. 1973

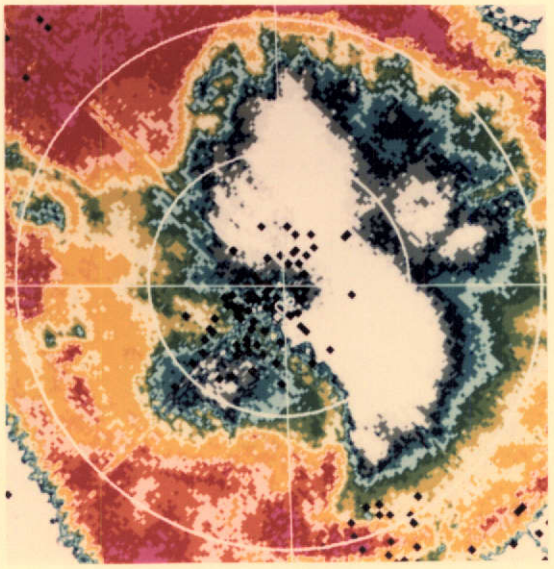

11 JULY 1973

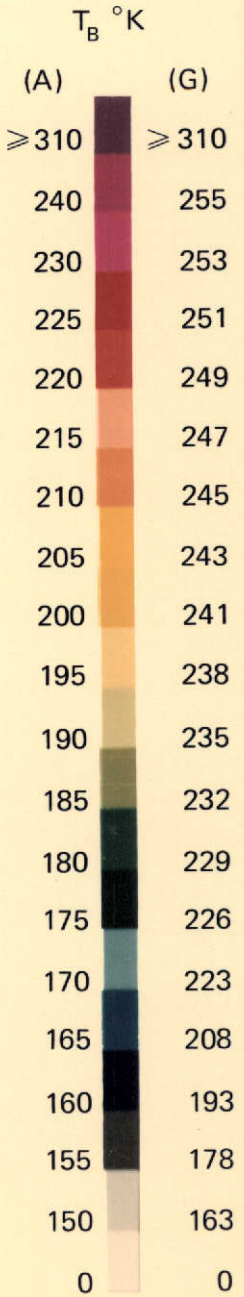

PLATE 7